buildings

MDPI

Article

Analyzing the Energy Flexibility Potential and Carbon-Emission Impacts of Solar–Air-Source Heat Pump Heating Systems for Nearly Zero-Energy Residential Buildings

Qing Wang [1], Hongxia Zhu [1], Jianan Qian [2], Pingxin Wang [1] and Shuqin Chen [2,*]

[1] Marketing Service Center (Metrology Center), State Grid Shandong Electric Power Company, Jinan 250000, China
[2] College of Civil Engineering and Architecture, Zhejiang University, Hangzhou 310058, China
* Correspondence: hn_csq@zju.edu.cn

Abstract

Against the background of China's dual carbon goals and the large-scale integration of renewable energy, building-side energy flexibility is of great significance for alleviating peak load pressure on the power grid, improving renewable energy accommodation, and reducing operational carbon emissions. This study investigates a nearly zero-energy residential building in the hot-summer and cold-winter climate zone of China. A TRNSYS-based dynamic model of a solar–air-source heat pump radiant floor heating system was developed to evaluate the effects of solar collector area, rated heat pump heating capacity, thermal storage tank volume, and heat pump start–stop center temperature on energy flexibility potential under the H1 strategy. Identified in the preceding study as having the greatest flexibility potential among the strategies evaluated, H1 switches off the heat pump throughout the peak period from 08:00 to 22:00, while solar heat and thermal energy stored in the tank provide space heating. Acceptable thermal comfort in all heated rooms was demonstrated under the reference configuration. A one-factor-at-a-time analysis and Spearman rank correlation analysis were conducted using two flexibility indicators: reduction in peak-period operating energy consumption and increase in solar heat collection relative to the corresponding baseline scenario. Peak-period carbon emissions were also evaluated. The collector area showed a strong negative association with peak-period electricity reduction ($\rho = -0.97$) and a strong positive association with increased solar heat collection ($\rho = 0.82$). The start–stop center temperature showed positive associations with both indicators, whereas the rated heating capacity and tank volume showed weaker associations. This study provides useful guidance for optimizing system configuration, reducing peak loads on the power grid, promoting renewable energy accommodation, and supporting the low-carbon operation of buildings.

Keywords: air-source heat pump; solar heating; influencing factors of energy flexibility; peak-period electricity reduction; carbon emission

Check for updates

Academic Editor: Constantinos A. Balaras

Received: 2 October 2026
Revised: 29 October 2026
Accepted: 30 October 2026
Published: 9 November 2026

Copyright: © 2026 by the authors. Licensee MDPI, Basel, Switzerland. This article is an open access article distributed under the terms and conditions of the Creative Commons Attribution (CC BY) license.

1. Introduction

China's dual-carbon goals and the rapid integration of wind and photovoltaic generation are increasing the need for flexible resources in the power system. Because renewable electricity generation is strongly influenced by weather conditions, its variability and uncertainty can intensify grid peak-shaving pressure and increase the demand for demand-side flexibility [1,2]. Flexible resources are essential for maintaining the safe and stable operation

of the new power system [3,4]. Building energy consumption accounts for a substantial share of end-use energy demand, representing approximately 30% of global energy consumption [5]. According to the International Energy Agency, space heating accounted for approximately half of residential energy consumption in 2021 [6].

Building energy flexibility is generally defined as the ability of a building or building energy system to adjust its energy demand or supply in response to local climate conditions, occupant requirements, and grid signals [7]. Energy flexibility can be achieved through load reduction, load shifting, peak-load management, thermal energy storage, and the coordinated operation of energy-conversion equipment [7]. Building heating loads possess thermal inertia and can be shifted in time [8]. By adjusting heat pump operating periods, thermal storage tank temperature, and heating-terminal operation, heating loads can be reduced, shifted, or stored without significantly compromising indoor thermal comfort, thereby enabling buildings to participate in demand response. Quantifying the flexibility potential of residential heating systems and converting it into a demand-side flexibility resource can help reduce the peak–valley difference of the power grid, improve renewable energy accommodation, and enhance grid resilience [9].

The development of nearly zero-energy buildings is an important pathway for achieving low-carbon transformation in the building sector [10,11]. Compared with conventional buildings, nearly zero-energy residences generally have more stable indoor thermal environments and greater thermal inertia and adjustment capacity, making them suitable flexible loads for interaction with the power grid [12]. Solar–air-source heat pump heating systems combine solar energy with air-source heat pumps to improve renewable energy utilization. Thermal storage tanks and the adjustable operation of heat pumps further enable demand response [13]. Existing studies have investigated solar–air-source heat pump heating systems, but most have focused on system performance optimization. Poppi et al. reported that an inappropriate match between collector area and storage capacity can increase the reliance on air-source heat pumps and reduce solar energy utilization [13]. Li et al. [14] proposed a time- and zone-partitioned solar–air-source heat pump heating system and showed that optimizing collector area, tank volume, and heat pump capacity can improve the solar fraction and reduce the duration of high-load heat pump operation. Wang et al. [15] reduced heat pump demand during peak periods by introducing nighttime charging and load-shifting strategies. Yan et al. [16] proposed an on-demand, time-partitioned heating strategy for a solar–air-source heat pump system and found that total energy consumption could be reduced by more than 20% while maintaining acceptable indoor-temperature fluctuations; lower tank operating temperatures also improved solar collection efficiency on the following day. Overall, existing studies have clarified the energy-efficiency and energy-saving benefits of these systems, but quantitative research on their energy flexibility potential remains limited, particularly regarding how key design and operating parameters affect flexibility.

Previous research [17] identified H1, in which the air-source heat pump is switched off from 08:00 to 22:00, as the strategy with the greatest flexibility potential when considering both peak-period electricity reduction and additional solar heat collection. Building on this finding, a solar–air-source heat pump radiant floor heating system model was established for a detached residential building in a hot-summer and cold-winter climate zone (HSCW) in China. Using the reduction in peak-period operating energy consumption and the increase in solar heat collection as indicators of energy flexibility potential, the effects of the solar collector area, rated heating capacity of the air-source heat pump, thermal storage tank volume, and heat pump start–stop center temperature on system flexibility and peak-period carbon emissions are investigated under the H1 strategy. The contributions of this study are as follows:

(1) Spearman rank correlation analysis was used to characterize the direction and strength of the associations between the investigated parameters and the two flexibility indicators, while peak-period carbon emissions were further evaluated to identify the main factors influencing the flexibility potential of the solar–air-source heat pump radiant floor heating system.

(2) The findings provide a reference for the design and operational control of heating systems in nearly zero-energy residential buildings, particularly in terms of coordinating solar collector area, heat pump capacity, thermal storage volume, and control settings to enhance peak-shaving capability and solar heat accommodation.

The remainder of this paper is organized as follows. Section 2 introduces the system model and research methods. Section 3 presents the case study, model validation, and simulation results. Section 4 discusses the findings and limitations. Section 5 summarizes the main conclusions.

2. Method

A dynamic simulation model of a solar–air-source heat pump radiant floor heating system is established in TRNSYS(v18). Collector area, rated heating capacity of the air-source heat pump, thermal storage tank volume, and the heat pump start–stop center temperature are selected as the key influencing factors. A one-factor-at-a-time method is used for comparative analysis. Energy flexibility potential is quantified using the ΔE and ΔQ; Spearman's rank correlation coefficient is further applied to identify the dominant influencing factors. The technical framework is shown in Figure 1.

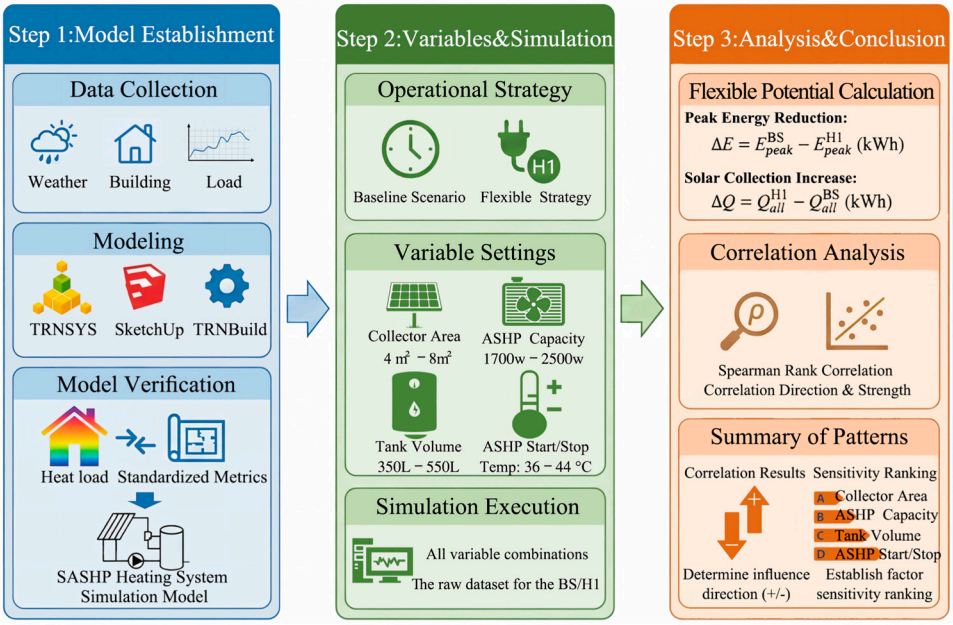


Figure 1. A flowchart for analyzing the factors influencing the energy flexibility of the solar–air-source heat pump radiant floor heating system.

2.1. Model of the Residential Solar–Air-Source Heat Pump Radiant Floor Heating System

To establish the operating model of the residential solar–air-source heat pump radiant floor heating system, the system configuration, equipment sizing, and operating-control settings were first determined.

As shown in Figure 2, the model consists of energy-production and energy-use subsystems. The energy-production subsystem comprises a flat-plate solar collector and an air-source heat pump connected in parallel. The heat collected by the solar collector and

the heat produced by the air-source heat pump are supplied independently to the thermal storage tank. The system has three operating modes: when solar heat is sufficient to meet the heating demand, the solar collector supplies heat alone and the heat pump remains off; when solar heat is insufficient, the solar collector and heat pump operate simultaneously; and when solar heat cannot be collected, the air-source heat pump operates alone to provide space heating. The energy-use subsystem is the indoor radiant floor heating terminal. A heating pump delivers hot water from the thermal storage tank to the building to meet the winter heating demand, while the hourly heating load of a typical detached residential building is obtained from EnergyPlus(v9.6.0) simulations.

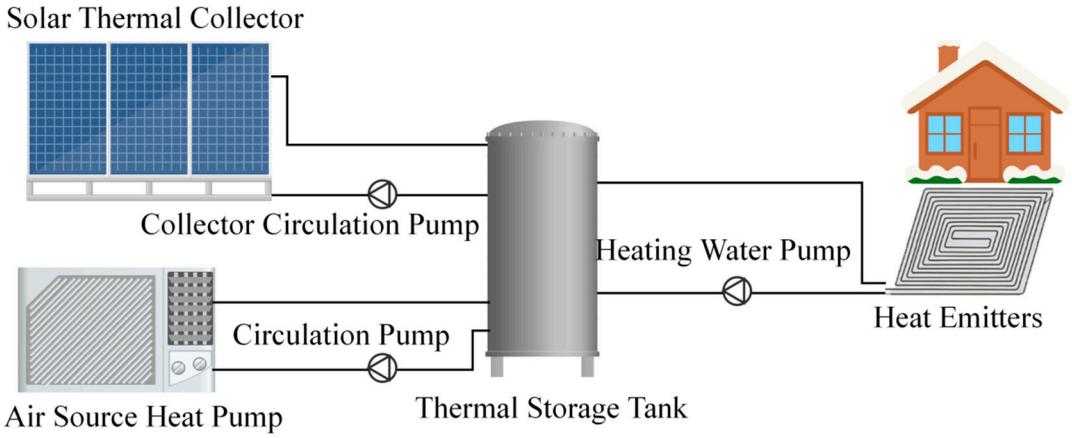


Figure 2. A schematic diagram of the solar–air-source heat pump radiant floor heating system.

The system sizing calculations include the solar collector area, air-source heat pump heating capacity, thermal storage tank volume, and supply and return water temperatures of the radiant floor heating system.

The solar collector is sized in accordance with GB 50495-2019, Technical Standard for Solar Water Heating and Space Heating Systems [18]. The collector tilt angle was set to the local latitude plus 10°, and the total collector area was calculated using the following equation:

$$A_C = \frac{86,400 Q_J f}{J_T \eta_{cd} (1 - \eta_L)} \quad (1)$$

where A_C is the total collector area (m^2); Q_J is the design load of the solar heating system (W); J_T is the average daily solar irradiance over 12 months on the collector aperture plane at the site ($J/(m^2 \cdot d)$); f is the solar fraction; η_{cd} is the collector's average heat collection efficiency based on the gross collector area; and η_L is the heat loss rate of the piping and thermal storage equipment [19].

The air-source heat pump is sized according to the building heating load, and its heating capacity is selected to meet the maximum heating demand. The volume of the thermal storage tank can be determined from the collector area; the recommended storage volume is 40–300 L per square meter of collector area [19]. The supply and return water temperatures of the radiant floor heating system are determined according to JGJ 142-2012 [20].

The operating logic of the system components was defined as follows. When the temperature difference between the solar collector outlet fluid and the water in the thermal storage tank exceeded 10 °C, the solar collector circulation pump was activated to charge the tank. When the temperature difference decreased below 2 °C, the circulation pump was switched off. The air-source heat pump was controlled according to the outlet water temperature on the load side of the thermal storage tank. The heat pump was switched on when the outlet temperature fell below 38 °C and switched off when it exceeded 42 °C.

When space heating was required, the heating circulation pump was activated, allowing the thermal storage tank to supply heat to the building [17].

Based on the system configuration, equipment-sizing results, operating-control logic, building envelope, and internal heat-gain settings, a dynamic operating model of the residential solar–air-source heat pump radiant floor heating system is established in TRNSYS. The model was used to simulate the operating characteristics of both the energy-supply and energy-use subsystems.

2.2. Selection of Factors Affecting System Energy Flexibility

To investigate the mechanisms through which key system parameters affect energy flexibility potential, four factors closely related to system operation were selected for analysis. Solar heat collection is primarily influenced by the solar collector area [21], whereas system operating energy consumption is closely associated with the rated heating capacity of the air-source heat pump [22]; The thermal storage tank volume affects water-temperature variations during the thermal storage process [23]; in addition, the heat pump start–stop temperature is an important operational parameter because it directly determines the heat pump operating duration and cycling frequency, thereby affecting the overall system energy consumption [24].

Accordingly, the effects of these four factors on the energy flexibility potential of the system were investigated using a one-factor-at-a-time approach. By varying one parameter while holding the remaining parameters constant, this approach facilitates the identification and interpretation of individual parameter effects on the flexibility indicators within the investigated ranges. The parameter ranges and corresponding system settings are summarized in Table 1. During the analysis of each individual factor, all other parameters were kept constant at the baseline values obtained from the equipment-sizing calculations described in Section 2.1. For each factor, the baseline value was taken as the central value, and additional values were selected symmetrically above and below it at equal intervals. Nine values were considered for each influencing factor. The solar collector area was varied at intervals of 1 m^2, the rated heating capacity of the air-source heat pump at intervals of 100 W, and the thermal storage tank volume at intervals of 25 L. The air-source heat pump start–stop center temperature was defined as the reference temperature for heat pump control. The heat pump was switched on when the tank outlet temperature fell 2 °C below the start–stop center temperature and switched off when it rose 2 °C above this temperature. Nine start–stop center temperatures were therefore considered at 1 °C intervals.

Table 1. The ranges of the influencing factors [18].

Influencing Factor	Values
Solar collector area/m^2	4, 5, 6, 7, 8, 9, 10, 11, 12
Rated heating capacity of the air-source heat pump/W	1700, 1800, 1900, 2000, 2100, 2200, 2300, 2400, 2500
Thermal storage tank volume/L	350, 375, 400, 425, 450, 475, 500, 525, 550
Air-source heat pump start–stop center temperature/°C	36, 37, 38, 39, 40, 41, 42, 43, 44

2.3. Evaluation Method for System Energy Flexibility Potential

To evaluate the system's capability for peak shaving and renewable energy accommodation, two indicators were adopted to quantify its energy flexibility potential. The reduction in peak-period operating energy consumption reflects the load-shifting capability of the system. It indicates the amount of energy consumption that can be reduced during the peak period under the H1 strategy compared with the corresponding baseline scenario (BS). The increase in solar heat collection reflects the system's ability to accommodate and utilize

additional renewable heat during flexible operation. It represents the renewable energy accommodation performance of the system. The two indicators describe complementary aspects of system operation under the H1 strategy. A larger ΔE indicates a greater reduction in peak-period electricity consumption relative to the corresponding BS, whereas a larger ΔQ indicates more solar heat collected relative to BS. Improvements in the two indicators do not necessarily occur simultaneously. For example, increasing the collector area may increase ΔQ while decreasing ΔE because it also lowers peak-period electricity consumption under BS. Based on the system operation model, the peak-period operating energy consumption and solar heat collection were simulated under different parameter settings.

The reduction in peak-period operating energy consumption (ΔE) is defined as:

$$\Delta E = E_{\text{peak}}^{\text{BS}} - E_{\text{peak}}^{\text{H1}} \tag{2}$$

where $E_{\text{peak}}^{\text{BS}}$ is the peak-period operating energy consumption under the baseline scenario before flexible regulation (kWh) and $E_{\text{peak}}^{\text{H1}}$ is the peak-period operating energy consumption after flexible regulation (kWh).

The increase in solar heat collection (ΔQ) is defined as:

$$\Delta Q = Q_{\text{all}}^{\text{H1}} - Q_{\text{all}}^{\text{BS}} \tag{3}$$

where $Q_{\text{all}}^{\text{H1}}$ is the solar heat collection after flexible regulation (kWh) and $Q_{\text{all}}^{\text{BS}}$ is the solar heat collection under the baseline scenario before flexible regulation (kWh).

2.4. Correlation Analysis of Influencing Factors

Spearman's rank correlation coefficient (ρ) measures the direction and strength of monotonic associations without requiring linear relationships or normally distributed variables. It was used to quantify the correlations between the system energy flexibility potential and four influencing factors: the solar collector area, rated heating capacity of the air-source heat pump, thermal storage tank volume, and air-source heat pump start–stop center temperature. The p-values were calculated using the asymptotic t-distribution approximation for Spearman's rank correlation coefficient, and the 95% confidence intervals were estimated using percentile bootstrap resampling.

Spearman's rank correlation coefficient was calculated as follows:

$$\rho = \frac{\sum_{i=1}^{n}(R_i - \bar{R})(S_i - \bar{S})}{\sqrt{\sum_{i=1}^{n}(R_i - \bar{R})^2 \sum_{i=1}^{n}(S_i - \bar{S})^2}} \tag{4}$$

where R_i and S_i are the ranks of the i^{th} observations of the two variables, respectively; $\bar{R}$ and $\bar{S}$ are their corresponding mean ranks; and n is the number of observations.

3. Case Simulation and Analysis

3.1. Simulation Model Development and Baseline Parameter Setting

This study focuses on a nearly zero-energy residential building in Hangzhou, located in the hot-summer and cold-winter (HSCW) climate zone. A solar–air-source heat pump radiant floor heating system model was established to investigate the factors influencing its energy flexibility potential. The region is characterized by cold and humid winters and hot and humid summers. As shown in Figure 3, the monthly average temperature in a typical year exhibits significant seasonal variation: the median temperature in winter is approximately 5.9 °C, with minimum values approaching −1 °C, while the median summer temperature reaches 27.0 °C, with maximum values exceeding 31 °C, resulting in an annual temperature difference of over 30 °C [25].

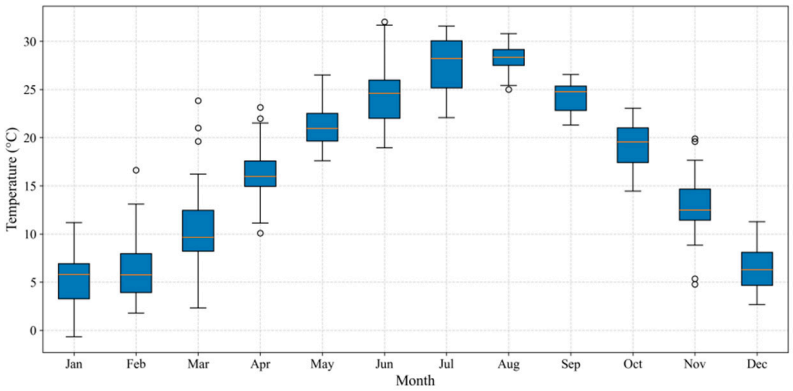
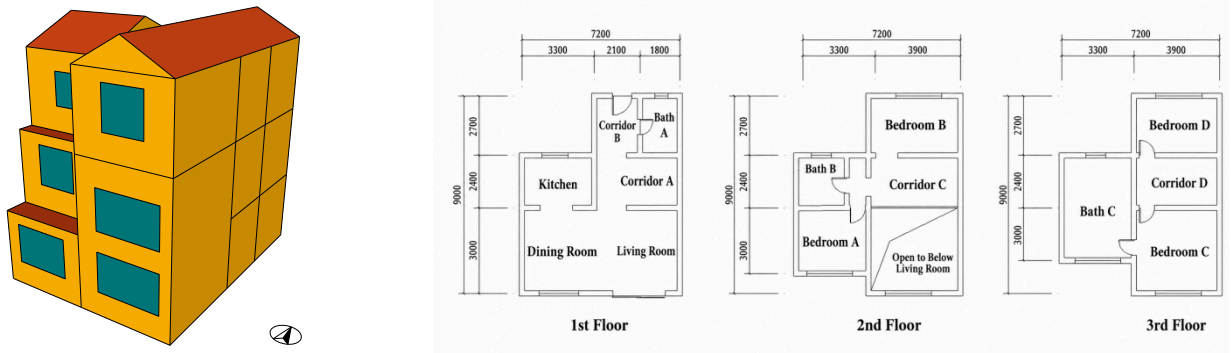


Figure 3. The monthly temperature distribution for a typical year [25].

A three-dimensional model of the case building was developed in SketchUp(v2024), as shown in Figure 4. The building-envelope parameters were specified in accordance with GB/T 51350-2019, Technical Standard for Nearly Zero Energy Buildings [26]. The heat transfer coefficient of the exterior walls, roof, interior walls, floor, and exterior windows were set to 0.4, 0.2, 1.2, 1.2, and 1.2 W/(m^2·K), respectively. The air change rate was set to 1.0 h^{-1} at an indoor–outdoor pressure difference of 50 Pa. Using the simplified empirical relationship $n_{inf} = n_{50}/20$, the infiltration air change rate used in the simulation was set to 0.05 h^{-1} [27]. Internal heat gains, heating setpoint temperatures, occupancy schedules and operating schedules were specified according to GB 55015-2021, General Code for Building Energy Efficiency and Renewable Energy Application [19], which is a current mandatory code for engineering construction in China. The heating season was defined as November 15 to April 3 of the following year. The heating setpoint temperature was 18 °C. The living room was heated from 07:00 to 20:00, while the bedrooms were heated from 20:00 to 07:00 on the following day. Based on these settings, EnergyPlus was used to simulate the annual hourly dynamic heating load of the building. The simulation used the China Standard Weather Data (CSWD) file for Hangzhou, Zhejiang Province, China (CHN_Zhejiang.Hangzhou.584570_CSWD.epw) [28]. The maximum heating load was 2083 W, and the annual heating energy demand was 7.66 kWh/(m^2·a), which satisfies the heating energy-efficiency requirement of 8 kWh/(m^2·a) for residential buildings in the HSCW climate zone [26].



(**a**) (**b**)

Figure 4. Case building model: (**a**) three-dimensional model; (**b**) floor plan.

The solar–air-source heat pump radiant floor heating system was sized using the method described in Section 2.1, and the resulting parameters were adopted as the baseline configuration. Based on the maximum building heating load of 2083 W, the solar collector area was determined to be 8 m^2. The rated heating capacity and rated input power of the

air-source heat pump were set to 2100 W and 700 W, respectively. According to empirical design recommendations for Hangzhou, approximately 56 L of storage volume can be allocated per square meter of solar collector area; accordingly, the thermal storage tank volume was set to 450 L. The top, side, and bottom heat loss coefficients of the thermal storage tank were each set to 2.3 kJ/(h·m^2·K). For radiant floor heating systems, the supply-water temperature should not exceed 60 °C, while the temperature difference between the supply and return water should generally remain between 5 and 10 °C. For residential buildings, a supply-water temperature of 35–45 °C is recommended. Accordingly, the supply-water temperature of the hydronic radiant floor heating system in this study was set to 40 °C. The rated mass flow rates of the solar collector, air-source heat pump, and radiant floor heating loops were set to 420, 360, and 400 kg/h, respectively. The building thermal model was configured in TRNBuild 3.0.294 and implemented using the Type 56 multizone building component in TRNSYS 18. The same building geometry, envelope thermal properties, occupancy schedules, and internal heat-gain assumptions were used in the EnergyPlus and Type 56 models. The radiant floor heating pipes were represented using the Active Layer function. A complete dynamic simulation model of the solar–air-source heat pump radiant floor heating system was then established by specifying the component input parameters, control logic, and interconnections. The TRNSYS simulation used a time step of 10 min, with both the integration and convergence tolerances set to 0.001.

To validate the developed TRNSYS model, an experimental validation was conducted. The measured and simulated values of the cumulative solar heat collection, air-source heat pump electricity consumption, collector circulation pump electricity consumption, and heating circulation pump electricity consumption over the 14-day test period were compared, as shown in Table 2. The relative differences between the simulated and measured values were within ±12% [29] for all indicators, indicating that the model can reasonably reproduce the main energy and electricity-consumption characteristics of the experimental system.

Table 2. Comparison between measured and simulated values during experimental period.

Parameter	Measured Value	Simulated Value
Solar heat collection (kWh)	31.77	28.06
Air-source heat pump electricity consumption (kWh)	28.10	24.75
Collector circulation pump electricity consumption (kWh)	4.09	4.29
Heating circulation pump electricity consumption (kWh)	5.38	5.68

A previous study [17] compared several flexible operation strategies involving indoor-temperature setpoints, floor thermal storage, solar heat collection control, thermal storage tank temperature, and heat pump start–stop control. The results showed that the H1 strategy had the greatest flexibility potential. During the heat pump shutdown period, the heat stored in the thermal storage tank continued to supply the radiant floor, while the thermal inertia of the floor structure helped slow the decline in indoor temperature. Figure 5 presents the heating-season indoor-temperature distributions of the heated rooms under the H1 strategy. All heated rooms remained above 14 °C and within the adaptive thermal-comfort range of 14–29 °C considered acceptable for occupants in the investigated climate region. Therefore, the H1 strategy was adopted in this study to investigate the effects of system parameters on energy flexibility.

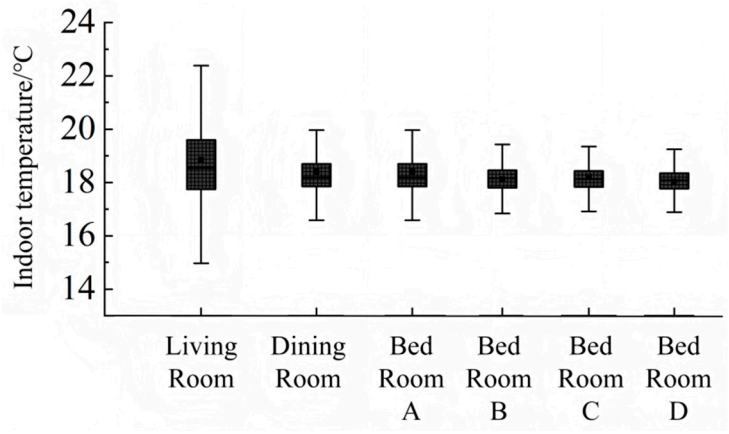
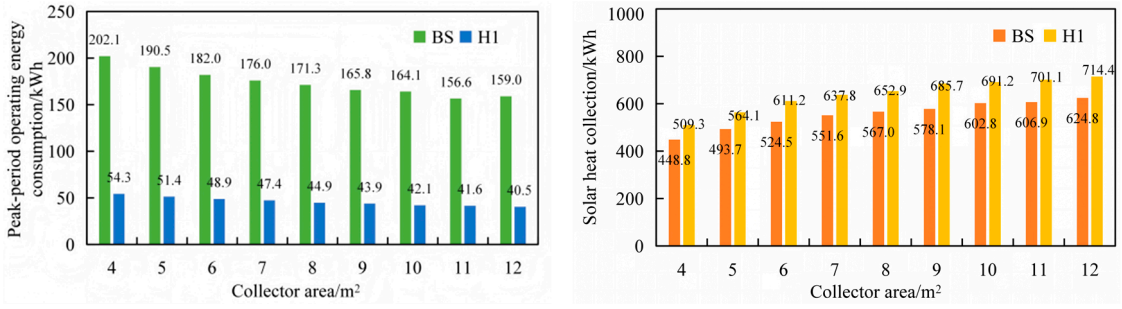


Figure 5. The indoor-temperature distributions of the heated rooms under the H1 strategy during the heating season.

3.2. Analysis of Factors Influencing System Energy Flexibility Potential

3.2.1. Collector Area

Figure 6 shows the cumulative peak-period operating energy consumption and solar heat collection of the system during the heating season under different collector areas. As the collector area increases, the peak-period operating energy consumption decreases under both the BS and the H1 strategy. When the collector area increases from 4 to 10 m^2, the peak-period operating energy consumption decreases from 202.1 to 164.1 kWh under the BS, corresponding to a reduction of 18.8%. Under the H1 strategy, it decreases from 54.3 to 42.1 kWh, corresponding to a reduction of 22.5%. This is because increasing the collector area enables the system to collect more solar energy, thereby reducing its dependence on the air-source heat pump and lowering energy consumption. Compared with the pronounced reduction in operating energy consumption under the BS as the collector area increases, the decrease under the H1 strategy is relatively smaller. This is because the peak-period operating energy consumption under the BS includes the energy consumption of both the air-source heat pump and the circulation pumps, whereas under the H1 strategy it consists only of the energy consumption of the circulation pumps. Since the latter has a lower energy-consumption base, the magnitude of variation is correspondingly smaller.



(**a**) (**b**)

Figure 6. Peak-period operating energy consumption and solar heat collection under different collector areas: (**a**) peak-period operating energy consumption; (**b**) solar heat collection.

Meanwhile, solar heat collection increases gradually with the collector area under both the BS and the H1 strategy. When the collector area increases from 4 to 10 m^2, solar heat collection increases from 448.8 to 602.8 kWh under the BS, representing an increase of 34.3%. Under the H1 strategy, it increases from 509.3 to 691.2 kWh, representing an increase of 35.7%. Increasing the collector area allows the system to collect more solar energy during

the daytime to meet the indoor-temperature requirements of the heated rooms. Compared with the pronounced increase in solar heat collection under the H1 strategy as the collector area increases, the increase under the BS is relatively smaller.

Based on the peak-period operating energy consumption and solar heat collection under the BS and H1 cases, the system energy flexibility potential under different collector areas was calculated using the evaluation indicators described in Section 2.3. Linear regression was then applied to obtain the best-fit lines, as shown in Figure 7. ΔE is negatively correlated with the collector area. As the collector area increases, the decrease in peak-period operating energy consumption under the BS is greater than that under the H1 strategy. ΔQ is positively correlated with the collector area, as indicated by the positive slope of the fitted line. This is because the increase in solar heat collection under the H1 strategy is greater than that under the BS.

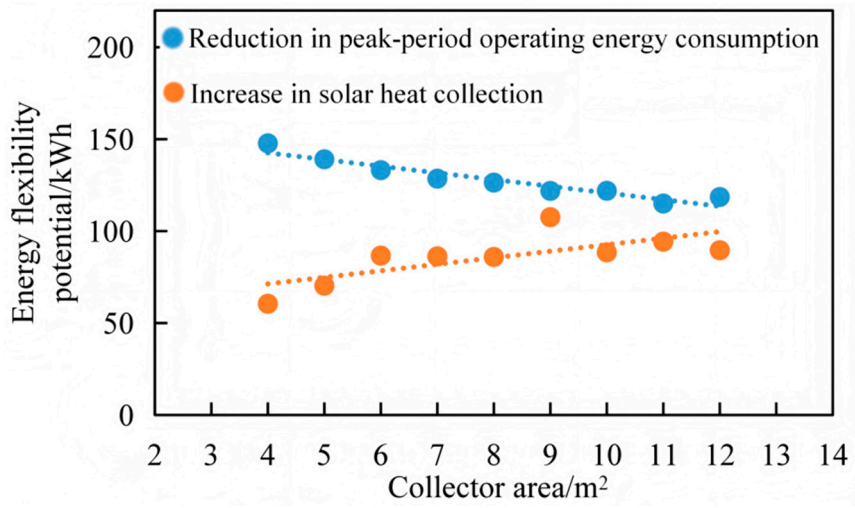


Figure 7. System energy flexibility potential under different collector areas.

3.2.2. Rated Heating Capacity of the Air-Source Heat Pump

Figure 8 shows the peak-period operating energy consumption and solar heat collection of the system during the heating season under different rated heating capacities of the air-source heat pump. As the rated heating capacity increases, both the peak-period operating energy consumption and solar heat collection generally decrease under the BS and H1 cases, although the magnitude of variation is relatively small. Under the BS, although the rated heating capacity of the air-source heat pump increases, the total building heating demand remains essentially unchanged, and the heating COP of the air-source heat pump remains constant at different rated capacities. Therefore, the total energy consumption of the heat pump changes only slightly, and the rated heating capacity has a limited effect on the peak-period operating energy consumption. Under the H1 strategy, the air-source heat pump does not operate during peak periods, and the peak-period operating energy consumption is mainly attributable to the circulation pumps. Therefore, variations in the rated heating capacity have only a limited direct effect on peak-period operating energy consumption, resulting in relatively small changes in the overall system energy consumption.

Based on the peak-period operating energy consumption and solar heat collection under the BS and H1 cases, the system energy flexibility potential under different rated heating capacities of the air-source heat pump was calculated and fitted, as shown in Figure 9 The fitted curves of the energy flexibility potential are relatively flat, indicating that the rated heating capacity of the air-source heat pump has a limited effect on the system energy flexibility potential.

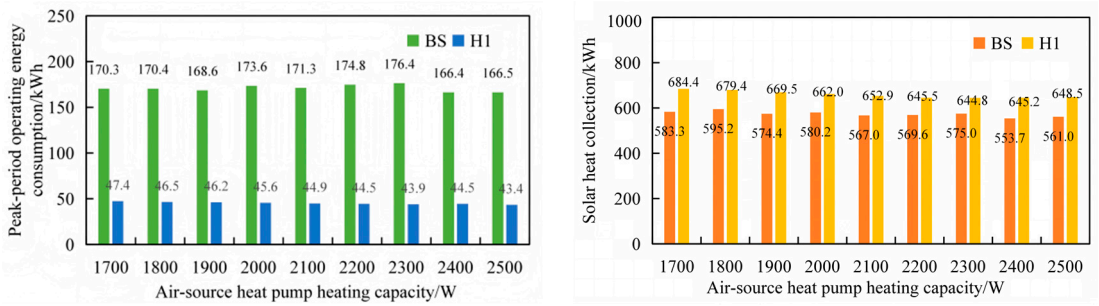


Figure 8. Peak-period operating energy consumption and solar heat collection under different rated heating capacities of the air-source heat pump: (**a**) peak-period operating energy consumption; (**b**) solar heat collection.

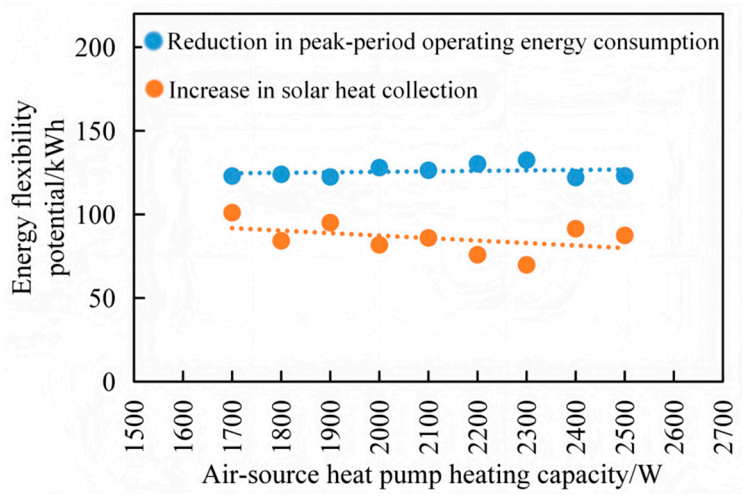


Figure 9. System energy flexibility potential under different rated heating capacities of the air-source heat pump.

3.2.3. Thermal Storage Tank Volume

Figure 10 shows the peak-period operating energy consumption and solar heat collection of the system during the heating season under different thermal storage tank volumes. As the tank volume increases, the changes in peak-period operating energy consumption under both the BS and H1 cases are relatively small, with no obvious variation trend. This is because the tank volume mainly affects the thermal storage capacity of the tank and the magnitude of water-temperature fluctuations, whereas the building heating load, rated heating capacity of the air-source heat pump, collector area, and system control logic remain unchanged. Therefore, changes in the tank volume have only a limited direct effect on the system's peak-period electricity demand.

Solar heat collection gradually increases with the tank volume under both the BS and H1 cases. When the tank volume increases from 350 to 550 L, solar heat collection increases from 497.2 to 634.2 kWh under the BS, corresponding to an increase of 137.0 kWh or 27.6%. Under the H1 strategy, it increases from 576.4 to 716.3 kWh, corresponding to an increase of 139.9 kWh or 24.3%. This is because increasing the tank volume enhances the thermal storage capacity of the system, allowing more solar energy collected during the daytime to be stored in the thermal storage tank to meet the indoor-temperature requirements of the heated rooms, thereby increasing the system's solar heat collection.

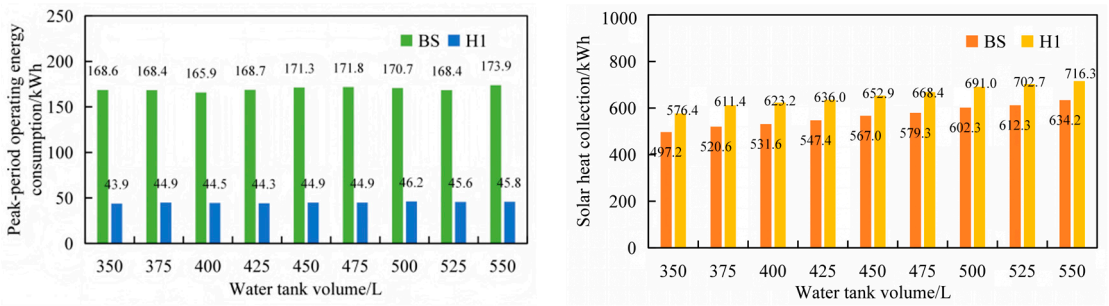


Figure 10. Peak-period operating energy consumption and solar heat collection under different thermal storage tank volumes: (**a**) peak-period operating energy consumption; (**b**) solar heat collection.

Based on the peak-period operating energy consumption and solar heat collection under the BS and H1 cases, the system energy flexibility potential under different thermal storage tank volumes was calculated and fitted, as shown in Figure 11. The fitted curves are relatively flat, indicating that the thermal storage tank volume has a limited effect on the system energy flexibility potential.

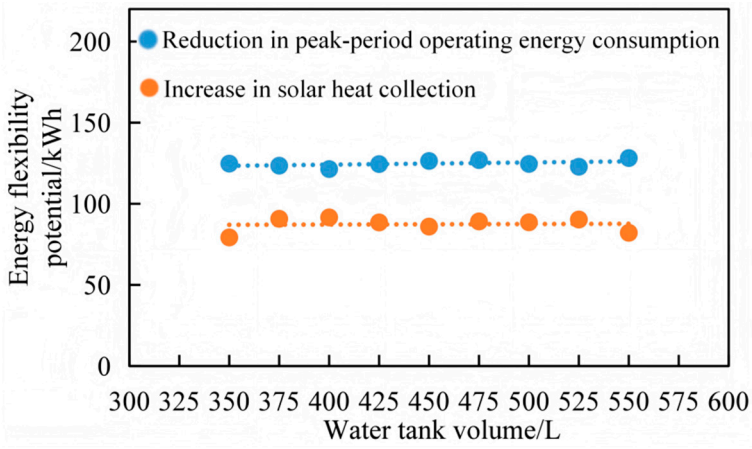


Figure 11. System energy flexibility potential under different thermal storage tank volumes.

3.2.4. Start–Stop Center Temperature of the Air-Source Heat Pump

Figure 12 shows the peak-period operating energy consumption and solar heat collection of the system during the heating season under different start–stop center temperatures of the air-source heat pump. As the start–stop center temperature increases, the peak-period operating energy consumption gradually increases under the BS, whereas it decreases under the H1 strategy. Under the BS, an increase in the start–stop center temperature causes the heat pump to start operation in a timely manner as the tank temperature decreases, thereby supplying additional heat to the tank. This increases the energy consumption of the heat pump and consequently increases the peak-period operating energy consumption. Under the H1 strategy, the heat pump does not operate during peak periods. However, the heat output of the heat pump during off-peak periods increases with the start–stop center temperature, allowing more heat to be stored in the thermal storage tank to meet the indoor-temperature requirements of the heated rooms. This reduces the demand for solar heat collection during peak periods and, consequently, lowers the operating energy consumption of the solar circulation pump, thereby reducing the peak-period operating energy consumption.

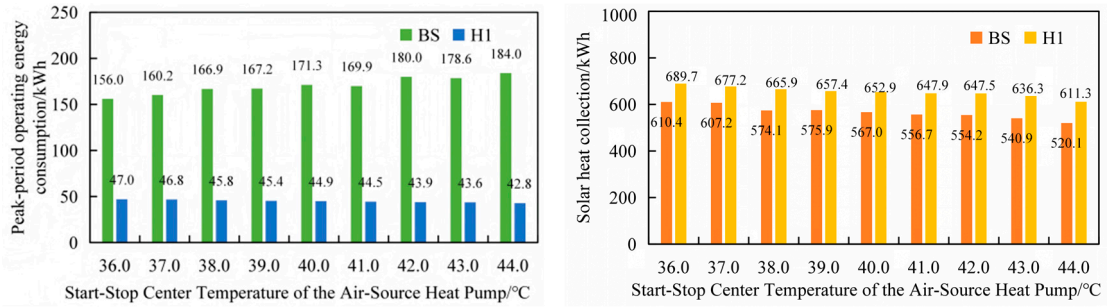


Figure 12. Peak-period operating energy consumption and solar heat collection under different start–stop center temperatures of the air-source heat pump: (**a**) peak-period operating energy consumption; (**b**) solar heat collection.

As the start–stop center temperature increases, solar heat collection under both the BS and H1 cases generally decreases. When the start–stop center temperature decreases from 44 to 36 °C, solar heat collection under the BS increases from 520.1 to 610.4 kWh, corresponding to an increase of 90.3 kWh or 17.4%. Under the H1 strategy, it increases from 611.3 to 689.7 kWh, corresponding to an increase of 78.4 kWh or 12.8%. This is because an increase in the start–stop center temperature causes the heat pump to provide more heat during off-peak periods, thereby maintaining a higher tank temperature. With a fixed temperature-difference criterion for solar circulation control, the solar heat transfer medium must reach a higher temperature during the peak period before the solar circulation loop can be activated, thereby reducing the system's solar heat collection.

Based on the peak-period operating energy consumption and solar heat collection under the BS and H1 cases, the system energy flexibility potential under different start–stop center temperatures was calculated and fitted, as shown in Figure 13. Both ΔE and ΔQ are positively correlated with the start–stop center temperature.

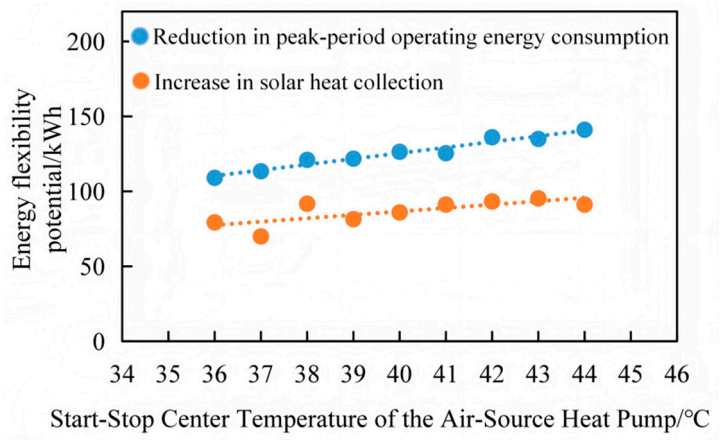


Figure 13. System energy flexibility potential under different start–stop center temperatures of the air-source heat pump.

3.3. Correlation Analysis Results

The Spearman rank correlation coefficient, *p*-value, and 95% bootstrap confidence intervals for the relationships between the two energy flexibility indicators and the four influencing factors are presented in Table 3.

For ΔE, the collector area and the start–stop center temperature show strong monotonic associations, with $\rho = -0.97$ and $\rho = 0.97$, respectively. Both associations have $p \leq 0.001$, and their 95% bootstrap confidence intervals do not include zero, indicating relatively stable

negative and positive associations within the investigated parameter ranges. The rated heating capacity and thermal storage tank volume show weak or moderate associations, with $p \geq 0.05$, and their confidence intervals include zero. Therefore, their monotonic associations are not statistically significant.

Table 3. Spearman correlation analysis of the influencing factors on system energy flexibility.

Indicators	Influencing Factors	Spearman ρ	*p*-Value	95% Bootstrap CI
Reduction in peak-period operating energy consumption	Solar collector area	−0.97	$p \leq 0.001$	[−0.9833, −0.6667]
	Rated heating capacity of the air-source heat pump	0.12	$p \geq 0.05$	[−0.5333, 0.9333]
	Thermal storage tank volume	0.35	$p \geq 0.05$	[−0.4671, 0.9500]
	Start–stop center temperature of the air-source heat pump	0.97	$p \leq 0.001$	[0.7333, 1.0000]
Increase in solar heat collection	Solar collector area	0.82	$p \leq 0.05$	[0.2667, 0.9837]
	Rated heating capacity of the air-source heat pump	−0.30	$p \geq 0.05$	[−0.8671, 0.5833]
	Thermal storage tank volume	−0.08	$p \geq 0.05$	[−0.7833, 0.8167]
	Start–stop center temperature of the air-source heat pump	0.68	$p \leq 0.05$	[0.0500, 1.000]

For ΔQ, the collector area shows a strong positive association ($\rho = 0.82$, $p \leq 0.05$), with a 95% bootstrap confidence interval of [0.2667, 0.9837]. The start–stop center temperature shows a positive association ($\rho = 0.68$, $p \leq 0.05$), with a 95% bootstrap confidence interval of [0.0500, 1.0000].

3.4. Impact of System Parameters on Peak-Period Carbon Emissions

During the operation of the solar–air-source heat pump radiant floor heating system, carbon emissions mainly arise from the indirect emissions associated with the electricity consumed by the air-source heat pump and circulation pumps. Therefore, peak-period operating energy consumption was converted into peak-period carbon emissions to evaluate the effects of different system parameters and operating strategies on carbon emissions.

The peak-period carbon emissions of the system can be expressed as:

$$C_{\text{peak}} = E_{\text{peak}} \times EF \tag{5}$$

where C_{peak} is the cumulative peak-period carbon emissions during the heating season (kg CO_2); E_{peak} is the cumulative electricity consumed by the air-source heat pump and circulation pumps during the peak period over the heating season (kWh); and EF is the electricity carbon-emission factor (kg CO_2/kWh). In this study, the average electricity-related carbon-emission factor for Zhejiang Province, China, in 2023 was adopted, with a value of 0.4974 kg CO_2/kWh [30].

The analysis of peak-period operational carbon emissions was conducted under the H1 scenario. The minimum investigated value range of each parameter was used as the baseline for comparing carbon emissions. For example, for the collector area ranging from 4 to 12 m^2, 4 m^2 was taken as the baseline.

Based on the H1 strategy, the effects of the four influencing factors on cumulative peak-period carbon emissions during the heating season were further analyzed. When the solar collector area increased from 4 to 10 m^2, the corresponding peak-period carbon emissions decreased from 27.01 to 20.94 kg CO_2, representing a reduction of 22.5%. This indicates

that increasing the collector area can improve solar energy utilization while reducing peak-period carbon emissions. When the rated heating capacity of the air-source heat pump increased from 1700 to 2500 W, the corresponding peak-period carbon emissions decreased from 23.58 to 21.59 kg CO_2, representing a reduction of 8.4%. This indicates that the rated heating capacity has a relatively limited effect on peak-period carbon emissions. When the thermal storage tank volume increased from 350 to 550 L, the corresponding peak-period carbon emissions increased from 21.84 to 22.78 kg CO_2, representing an increase of 4.3%. This indicates that increasing the tank volume primarily enhances the system's thermal storage capacity and solar heat utilization rather than directly reducing the carbon emissions associated with peak-period energy consumption. When the start–stop center temperature of the air-source heat pump increased from 36 to 44 °C, the corresponding peak-period carbon emissions decreased from 23.38 to 21.29 kg CO_2, representing a reduction of 8.9%. This indicates that increasing the start–stop center temperature can further reduce peak-period carbon emissions under the H1 strategy. This reduction occurs because the heat pump stores more thermal energy in the tank during off-peak periods, thereby reducing system energy consumption and the associated carbon emissions during peak periods.

Overall, the four influencing factors have different effects on peak-period carbon emissions. The solar collector area exerts the strongest carbon-reduction effect, mainly by increasing the contribution of solar energy and thereby reducing peak-period energy consumption. The start–stop center temperature of the air-source heat pump has the second-strongest effect, primarily by shifting part of the heat pump operation to off-peak periods. In contrast, the rated heating capacity of the air-source heat pump and the thermal storage tank volume have relatively limited effects on peak-period carbon emissions.

4. Discussion

4.1. Significance

This study analyzes the energy flexibility characteristics of a solar–air-source heat pump radiant floor heating system from the perspectives of both system design and operational control. The results show that the solar collector area and the start–stop center temperature of the air-source heat pump show relatively strong monotonic associations with the system energy flexibility indicators within the investigated parameter ranges. In contrast, the rated heating capacity of the air-source heat pump and the thermal storage tank volume show weaker and statistically non-significant associations. These findings indicate that, for nearly zero-energy residential buildings, system flexibility is not determined solely by equipment capacity, but is more strongly influenced by the coordination of solar energy supply, thermal storage processes, and heat pump operational control.

Increasing the solar collector area can reduce the system's absolute energy consumption during peak periods. However, it also reduces the peak load under the baseline condition, thereby narrowing the additional peak-shaving potential that can be released through flexibility control. This indicates that improvements in energy efficiency and energy flexibility do not necessarily occur simultaneously. Therefore, the evaluation of energy flexibility should consider both the absolute peak-period load and the adjustable load relative to the baseline condition.

The start–stop center temperature of the air-source heat pump reflects a trade-off between solar energy utilization and load shifting. A lower start–stop center temperature helps reduce the tank temperature and creates more favorable conditions for solar heat collection, whereas a higher start–stop center temperature increases the amount of heat stored by the heat pump during off-peak periods, thereby reducing energy consumption during peak periods. Therefore, the start–stop center temperature is not only a conventional

operating parameter but also an important flexibility-control variable for coordinating solar energy utilization and load shifting.

Although increasing the thermal storage tank volume improves the physical thermal storage capacity of the system, it does not lead to a corresponding increase in energy flexibility. This indicates that thermal storage capacity can be effectively converted into dispatchable demand-side flexibility only when combined with appropriate charging and discharging control. Overall, for nearly zero-energy residential buildings, system flexibility depends less on equipment capacity alone and more on the coordination of solar energy supply, thermal storage processes, and heat pump operational control.

4.2. Limitations

This study has several limitations. First, the investigated building is a representative nearly zero-energy detached residence located in the hot-summer and cold-winter climate zone. The identified effects of the investigated parameters are influenced by the building's thermal characteristics, climatic conditions, and local solar energy resources. Therefore, the applicability of the results to other climate zones and building types requires further validation. Second, the one-factor-at-a-time method was used to analyze the independent effects of individual parameters, and the interactions among the solar collector area, heat pump capacity, thermal storage tank volume, and operational control parameters were not considered. A constant COP was also assumed for all investigated heat pump capacities, without accounting for efficiency variations associated with outdoor temperature, water temperature, or part-load operation. In addition, the H1 strategy assumes that the air-source heat pump is switched off during a fixed peak period. This assumption does not fully reflect the dynamic variations in actual grid demand and meteorological conditions. Consequently, the strategy may not fully capture the system's flexibility-regulation capability under dynamic demand-response conditions, and the simulated operating performance may differ from that observed in practical applications. In real residential buildings, implementation may also be affected by occupant thermal-comfort requirements, differences in building thermal inertia and communication delays. These factors may limit the direct application of the fixed H1 strategy. The economic feasibility of the investigated configurations and the H1 strategy was not assessed. Therefore, improvements in energy flexibility should not be interpreted as evidence of economic benefits, which also depend on equipment investment, operating electricity costs, and potential demand-response incentives. Furthermore, the carbon-emission calculations were based on an annual average electricity emission factor and did not account for hourly variations in grid carbon intensity or differences between peak and off-peak electricity generation [31]. Therefore, the carbon-emission results obtained in this study mainly reflect the average emission effects associated with changes in peak-period energy consumption under different parameter settings.

5. Conclusions

This study investigated a nearly zero-energy detached residence located in the hot-summer and cold-winter climate zone and analyzed the effects of key parameters of a solar–air-source heat pump radiant floor heating system on its energy flexibility potential and peak-period carbon emissions. The main conclusions are as follows:

(i) The collector area and the start–stop center temperature show the strongest monotonic associations with ΔE, with Spearman coefficients of −0.97 and 0.97, respectively. When the collector area increases from 4 to 10 m^2, the peak-period operating energy consumption under the H1 strategy decreases by 22.5%.

(ii) The collector area shows the strongest monotonic association with the increase in solar heat collection, with a Spearman coefficient of 0.82, followed by the start–stop

center temperature, with a coefficient of 0.68. When the start–stop center temperature decreases from 44 to 36 °C, the solar heat collection under the H1 strategy increases by 12.8%.

(iii) The solar collector area and the start–stop center temperature of the air-source heat pump are the primary parameters affecting peak-period carbon emissions. Under the H1 strategy, increasing the collector area reduces peak-period carbon emissions by 22.5%, whereas increasing the start–stop center temperature reduces them by 8.9%.

Future research could extend the analysis to different climate zones and building types to investigate how system flexibility varies under different building-load and solar-resource conditions. The one-factor-at-a-time analysis could also be extended to multi-parameter joint optimization to further clarify the interactions between design parameters and operational control parameters. With respect to operational control, dynamic control of the air-source heat pump start–stop temperature and the thermal storage state of the tank could be implemented by incorporating solar-radiation forecasts, building-load forecasts, dynamic electricity prices, and grid demand signals [32,33]. A comprehensive scheduling study could also be conducted to analyze the complete load-shifting process, including peak-period, off-peak, and total electricity consumption, nighttime reheating, heat delivered indoors, storage losses, and changes in stored energy. A closed energy balance could then be established to evaluate the overall performance of the load-shifting strategy. In addition, hourly electricity carbon-emission factors could be introduced to enable a more accurate assessment of the carbon-emission impacts of different operating strategies. Economic feasibility could also be evaluated by considering equipment investment, operating electricity costs under time-of-use tariffs, and potential demand-response incentives, thereby clarifying the trade-offs between energy flexibility and economic performance.

Overall, this study identifies the main parameter associations with the energy flexibility potential of the investigated solar–air-source heat pump radiant floor heating system. For the nearly zero-energy detached residential building in the hot-summer and cold-winter climate zone of China, the results clarify how the considered design and control parameters are related to reductions in peak-period operating energy consumption and solar heat accommodation under the H1 strategy. These findings provide a reference for the parameter selection and operational control of similar residential heating systems and may support their participation in building-side demand-response applications.

Author Contributions: Conceptualization, S.C.; Methodology, H.Z., J.Q. and S.C.; Software, Q.W. and H.Z. Validation, Q.W. and J.Q.; Formal analysis, Q.W., H.Z., J.Q. and P.W.; Investigation, H.Z. and J.Q.; Resources, Q.W., H.Z., J.Q. and P.W.; Data curation, H.Z. and J.Q.; Writing—original draft, Q.W., H.Z., J.Q. and P.W.; Writing—review & editing, S.C.; Visualization, P.W.; Supervision, S.C.; Project administration, S.C.; Funding acquisition, S.C. All authors have read and agreed to the published version of the manuscript.

Funding: This work was supported by the Science and Technology Project of State Grid Shandong Electric Power Company under Grant No. 520633250009.

Data Availability Statement: The simulation data supporting the findings of this study are available from the corresponding author upon reasonable request.

Conflicts of Interest: Qing Wang, Hongxia Zhu, and Pingxin Wang are employed by the Marketing Service Center (Metrology Center), State Grid Shandong Electric Power Company. The remaining authors declare that the research was conducted in the absence of any commercial or financial relationships that could be construed as a potential conflict of interest. The authors declare that this study received funding from the Science and Technology Project of State Grid Shandong Electric Power Company under Grant No. 520633250009. The funder was not involved in the study design,

collection, analysis, or interpretation of data; the writing of this article; or the decision to submit it for publication.

References

1. Chen, S.; Huang, Y.; Hu, J.; Yang, S.; Lin, C.; Mao, K.; Chen, Y. Characterizing energy-related occupant behavior towards urban residential buildings in China with statistical database establishment. *Energy Build*. **2024**, *324*, 114889. [CrossRef]
2. Gomaa, M.M.; Mardenli, D.H.; Alaidroos, A.; Berkouk, D.; Bouzir, T.A.K.; Ragab, A. CFD-driven passive cooling and renewable retrofits for nearly net-zero university buildings in a hot-humid climate. *Buildings* **2026**, *16*, 3654. [CrossRef]
3. Feng, S.; Shi, X.; Zheng, Y.; Shi, F. Evaluation methods and improvement measures for power-system flexibility considering renewable-energy uncertainty. *Shandong Electr. Power* **2025**, *52*, 32–43.
4. Zhang, J.; Pan, S.; Hu, C.; Liu, H.; Wang, X. Optimal scheduling strategy for microgrids based on a hierarchical demand-response mechanism. *Shandong Electr. Power* **2025**, *52*, 88–99.
5. International Energy Agency. *Energy Efficiency 2025*; International Energy Agency: Paris, France, 2025.
6. International Energy Agency. *The Future of Heat Pumps*; OECD Publishing: Paris, France, 2022.
7. Huang, Y.; Chen, S.; Qian, J.; Li, J.; Lu, F.; Nord, N.; Kuznik, F. An uncertainty-based energy flexibility potential prediction approach for air conditioners in a residential community. *Energy* **2026**, *360*, 141614. [CrossRef]
8. Gür, M.; Öztop, H.F. PV/T-assisted underfloor heating with phase change material to improve indoor thermal comfort in a test room designed according to nearly zero-energy building principles: Experimental and numerical study. *Int. Commun. Heat Mass Transf.* **2026**, *180*, 112730. [CrossRef]
9. Cui, C.; Zhang, J.; Yu, C.; Shi, X. Optimal scheduling of electric heating loads for medium- and high-voltage distribution-network security. *Shandong Electr. Power* **2026**, *53*, 97–106.
10. Xue, Y.; Xiao, J.; Fan, Y.; Gao, T.; Ge, J. Research progress on heat and moisture transfer in building envelopes for zero-energy buildings. *J. Zhejiang Univ. Eng. Sci.* **2026**, *60*, 1148–1165.
11. Gür, M.; Öztop, H.F.; Hepbasli, A. When net-zero falls short of carbon neutrality: Assessing dynamic life-cycle carbon integrity in grid-connected building microgrids. *Sustain. Cities Soc.* **2026**, *149*, 107843. [CrossRef]
12. Foteinaki, K.; Li, R.; Heller, A.; Rode, C. Heating system energy flexibility of low-energy residential buildings. *Energy Build.* **2018**, *180*, 95–108. [CrossRef]
13. Poppi, S.; Sommerfeldt, N.; Bales, C.; Madani, H.; Lundqvist, P. Techno-economic review of solar heat pump systems for residential heating applications. *Renew. Sustain. Energy Rev.* **2018**, *81*, 22–32. [CrossRef]
14. Li, T.; Liu, Q.; Gong, Y.; Xia, J.; Shi, L.; Mao, Q. Collaborative optimization of solar-assisted air source heat pump temporal-spatial partitioned heating system in HSCW zone of China. *Energy Build.* **2023**, *299*, 113601. [CrossRef]
15. Wang, Y.; Quan, Z.; Zhao, Y.; Wang, L.; Liu, Z. Performance and optimization of a novel solar-air source heat pump building energy supply system with energy storage. *Appl. Energy* **2022**, *324*, 119706. [CrossRef]
16. Yan, X.; Yu, P.; Wang, D. Flexible energy-saving control strategy for solar and air-source heat pump combined heating based on demand-based time-partitioned operation. *Distrib. Energy* **2023**, *8*, 1–10.
17. Chen, S.; Gao, Y.; Huang, Y.; Xingxing, Z.; Lin, X.; Zhong, W. Energy flexibility potential analysis of solar-air source heat pump heating systems for nearly zero-energy residential buildings in hot-summer and cold-winter regions. *Acta Energiae Solaris Sin.* **2026**, *47*, 167–174.
18. *GB 50495-2019*; Technical Standard for Solar Heating and Space Heating Engineering. China Architecture & Building Press: Beijing, China, 2019.
19. *GB 55015-2021*; General Code for Building Energy Conservation and Renewable Energy Utilization. China Architecture & Building Press: Beijing, China, 2021.
20. *JGJ 142-2012*; Technical Specification for Radiant Heating and Cooling. China Architecture & Building Press: Beijing, China, 2012.
21. Xu, B.; Wang, S.; Chen, Z.; Xu, Z.; Chen, X. Design and optimization of a seasonal solar thermal-storage system for small buildings. *J. Eng. Thermophys.* **2024**, *45*, 1671–1678.
22. Zhu, C. Capacity Matching and Operation Synchronization Optimization of a Solar and Air-Source Heat Pump Combined Heating System. Master's Thesis, Xi'an University of Architecture and Technology, Xi'an, China, 2019.
23. Zhang, Y.; Cui, H.; Wang, C.; Wang, C.; Chen, H. Comparative analysis of a solar-ground-source heat pump heating system with phase-change thermal storage based on TRNSYS. *Acta Energ. Sol. Sin.* **2025**, *46*, 579–586.
24. Wang, X.; Rao, Z.; Sun, W.; Cao, X. Control strategy for a solar and air-source heat pump combined hot-water supply system. *Sol. Energy* **2016**, *54–59*, *77*.
25. Chen, S.; Qian, J.; Luo, J.; Ye, S.; Liu, Y.; Ge, J. Short-term park cooling load prediction based on CNN-GRU-SAO-MHA hybrid model integrating equipment operation features. *Int. J. Green Energy* **2026**, *23*, 2524–2538. [CrossRef]
26. *GB/T 51350-2019*; Technical Standard for Nearly Zero Energy Buildings. China Architecture & Building Press: Beijing, China, 2019.

27. Van Den Bossche, N. *Building Envelope Airtightness*; IEA EBC Annex 74; Ghent University: Ghent, Belgium, 2020.
28. Energy Models. CHN_Zhejiang.Hangzhou.584570_CSWD.epw: China Standard Weather Data for Hangzhou, Zhejiang Province, China. Available online: https://energy-models.com/content/chnzhejianghangzhou584570cswdzip (accessed on 24 October 2026).
29. Liu, P. Operation Optimization of a Multi-Source Coupled Heating System Based on an Air-Source Heat Pump. Master's Thesis, Northeast Electric Power University, Jilin, China, 2023.
30. Ministry of Ecology and Environment of the People's Republic of China. 2023 Electricity Carbon Dioxide Emission Factors. Available online: https://www.mee.gov.cn/xxgk2018/xxgk/xxgk01/202512/W020251231726284332528.pdf (accessed on 24 October 2026).
31. Gür, M.; Öztop, H.F. Year-round experimental 4E assessment of an integrated PV/T-BIPV system in an nZEB-oriented test building. *Sci. Rep.* **2026**. [CrossRef]
32. Salem, K.M.; Elgharib, A.O.; Rey-Hernández, J.M.; Rey-Martínez, F.J. A generalizable hybrid AI-LSTM model for energy consumption and decarbonization forecasting. *Sustainability* **2025**, *17*, 10882. [CrossRef]
33. Salem, K.M.; Rey-Martínez, F.J.; Elgharib, A.O.; Rey-Hernández, J.M. Decarbonizing the built environment: An AI-powered framework for predictive energy planning. *Earth Syst. Environ.* **2026**, *10*, 9767–9790. [CrossRef]

Disclaimer/Publisher's Note: The statements, opinions and data contained in all publications are solely those of the individual author(s) and contributor(s) and not of MDPI and/or the editor(s). MDPI and/or the editor(s) disclaim responsibility for any injury to people or property resulting from any ideas, methods, instructions or products referred to in the content.